RSC Advances

PAPER

View Article Online
View Journal | View Issue

Cite this: *RSC Adv.*, 2016, **6**, 25427

An electrochemical biosensing platform based on 1-formylpyrene functionalized reduced graphene oxide for sensitive determination of phenol†

Zulin Hua, Qin Qin, Xue Bai,* Xin Huang and Qi Zhang

Received 23rd December 2015
Accepted 1st March 2016

DOI: 10.1039/c5ra27563f

www.rsc.org/advances

A highly efficient enzyme-based screen printed electrode (SPE) was developed based on the covalent immobilization of tyrosinase (Tyr) on 1-formylpyrene (1-FP) functionalized reduced graphene oxide (rGO). Here, the bifunctional molecule 1-FP was assembled onto rGO sheets. Subsequently, a Tyr molecule was immobilized on the 1-FP forming a biocompatible nanocomposite, which was further coated onto the working electrode surface of the SPE. The performance of as-prepared biosensor was investigated by the detection of phenol in the presence of molecular oxygen. Wide linear range, low detection limit and high sensitivity were obtained with this biosensor due to the good conductivity of rGO as well as the high bioactivity of Tyr well retained by the 1-FP/rGO platform. Finally, the proposed biosensor was successfully employed for the detection of phenol in real water samples with satisfactory results. These findings suggest that this novel biosensor could offer great potential for rapid, cost-effective and on-field analysis of phenolic compounds.

1. Introduction

Phenol and its derivatives are widespread contaminants whose sources are both natural and industrial. Phenol is massively used in the production of plastics, fertilizer, paint, rubber, adhesives, paper and soap.[1,2] Due to its high toxicity and low degradation, excess concentrations of phenol in the environment would cause environmental problems as well as human disease.[3] Therefore, sensitive detection of phenol is of great importance for the protection of public health and the environment.

Various approaches, such as high performance liquid chromatography (HPLC),[4] UV-Vis spectrophotometry,[5] flame ionization detection,[6] *etc.* have been developed for the detection of phenol. In fact, these methods are associated with certain disadvantages, such as high cost, special instrumentation, complicated sample pretreatment, unstable detection results, and unsuitable on-site monitoring.[7,8] For this reason, immense efforts have been focused on the development of simple and effective analytical methods for fast determination of phenol. Amperometric biosensors based on enzymes have been proven to be promising for this purpose due to their easy operation, fast response and feasibility of miniaturization.[9–11]

Tyrosinase (Tyr) is a well-known multicopper-oxidase enzyme that could catalyze the oxidation of various phenolic compounds with the concomitant reduction of oxygen.[12,13] Thus, biosensors based on Tyr have been studied extensively for phenol determination. The main problem in constructing such an enzyme based biosensor is the effective immobilization of enzyme molecules onto electrode surface.[14–16] Various methods have been reported for the immobilization of enzyme on suitable matrix, such as adsorption,[17,18] covalent binding,[19,20] entrapment[21,22] and encapsulation.[23,24] Among these methods, covalent attachments to electrochemical materials have been frequently used for enzyme immobilization due to the enzyme stability as well as the high immobilizing efficiency. In most studies of covalent immobilization, the key point is to introduce functional groups onto the electrochemical materials which could further interact with enzyme (usually the amino groups). For example, Pang *et al.*[25] used 1-aminopyrene to functionalize carbon nanotubes (CNTs) *via* π–π interaction, then the functionalized CNTs was linked to one aldehyde group of glutaraldehyde, leaving the other aldehyde group of glutaraldehyde flexible to interact with laccase. Wei *et al.*[26] applied 1-pyrenebutanoic acid, succinimidyl ester (PASE) as the noncovalent functionalization reagent adsorbing onto the graphene oxide (GO) *via* π–π interaction, then Tyr was covalently bind with PASE-functionalized GO by forming amide bond. However, some of these procedures are relatively complicated, or require the use of organic solvents, which would lead to relatively poor stability and bioactivity of enzyme. Thus, searching for a simple and reliable scheme to immobilize enzyme is of considerable interest.

Key Laboratory of Integrated Regulation and Resource Development on Shallow Lake of Ministry of Education, College of Environment, Hohai University, Nanjing 210098, China. E-mail: baixue@hhu.edu.cn; Tel: +86 15951940543

† Electronic supplementary information (ESI) available. See DOI: 10.1039/c5ra27563f

Screen printed electrodes (SPEs), for their especially low cost, fast response and large-scale production, have been widely used in sensors.[27,28] Regardless of these advantages, signal conductivity remains a weak point of SPE electrodes. To solve this problem, various materials such as carbon nanomaterials,[29,30] metal nanoparticles[31,32] and polymers[33,34] have been used to modify SPEs. Graphene,[35,36] a two-dimensional carbon atom monolayer, exhibits good mechanical strength, large specific surface area, and excellent electronic properties, making it a promising electrode modifier. Besides, due to its unique nanostructure of six-membered rings, various π-conjugative structured materials, such as benzenes,[37] pyrenes[38] and heteroaromatic compounds[39] have been used to interact with graphene through π–π stacking interaction, providing spacer chains terminated with flexible functional groups onto graphene surface. Though graphene possesses those outstanding characteristics, it suffers from very limited water-dispersing ability,[40,41] which would exert hurdles for the fabrication of the enzyme-based electrodes. Thus, reduced graphene oxide (rGO) is a much more attractive material for enzyme immobilization due to its enhanced dispersion ability as well as good electrical properties.[42]

1-Formylpyrene (1-FP) is a bifunctional molecule with a pyrenyl group and a aldehyde group. The pyrenyl group of 1-FP, being highly aromatic in nature, can interact strongly with graphene sheets *via* π–π stacking. By functionalization of graphene with 1-FP, lots of aldehyde groups can be introduced uniformly on the graphene surface and can be further used to immobilize enzymes to construct biosensors. However, to the best of our knowledge, there was no studies on the immobilization of enzymes using 1-FP functionalized graphene by far.

In this paper, we applied 1-FP to functionalize rGO for Tyr immobilization (Scheme 1). The obtained Tyr-1-FP/rGO biocomposite was then coated on the SPE surface through a drop casting method. The non-covalent functionalization of rGO with 1-FP was identified by Fourier transform infrared spectroscopy (FTIR). The Tyr-1-FP/rGO composite was fully characterized by X-ray photoelectron spectroscopy (XPS) and electrochemical impedance spectroscopy (EIS). The amperometric response of the prepared enzyme electrode in the detection of phenol was investigated. The results showed that the developed biosensor exhibited good stability and high sensitivity for the detection of phenol.

2. Experimental

2.1. Reagents and materials

Tyr (EC 1.14.18.1 from mushroom) and phenol were purchased from Sigma-Aldrich (USA). 1-FP was bought from Aladdin (Shanghai, China). GO was obtained from Nanjing XFNano Materials Tech Co., Ltd. A 0.1 M phosphate buffer solution (PBS) made from Na_2HPO_4 and NaH_2PO_4 was employed as the supporting electrolyte. Absolute ethanol was used as rGO dispersant agent. Na_2HPO_4, NaH_2PO_4 and absolute ethanol were all obtained from Sinopharm Chemical Reagent Co., Ltd. (Shanghai, China). Deionized water obtained with a Milli-Q System (Billerica, MA, USA) was used for preparing all solutions. All reagents were of analytical grade and were used as received without further purification.

2.2. Apparatus and electrodes

All the electrochemical experiments were carried out using a CHI 660E electrochemical workstation (Shanghai Chenhua Instrument Co. Ltd, China). A three-electrode system, consisting of the modified SPE (diameter, 3 mm) as the working electrode, a platinum wire as the counter electrode, and a saturated Ag/AgCl electrode as the reference electrode, was employed. The FT-IR spectra of rGO, 1-FP and 1-FP/rGO were collected between 4000 and 500 cm^{-1} (Mid infrared region) on a Nicolet Nexus Avater 370 FTIR spectrophotometer (Nicolet, USA), with 256

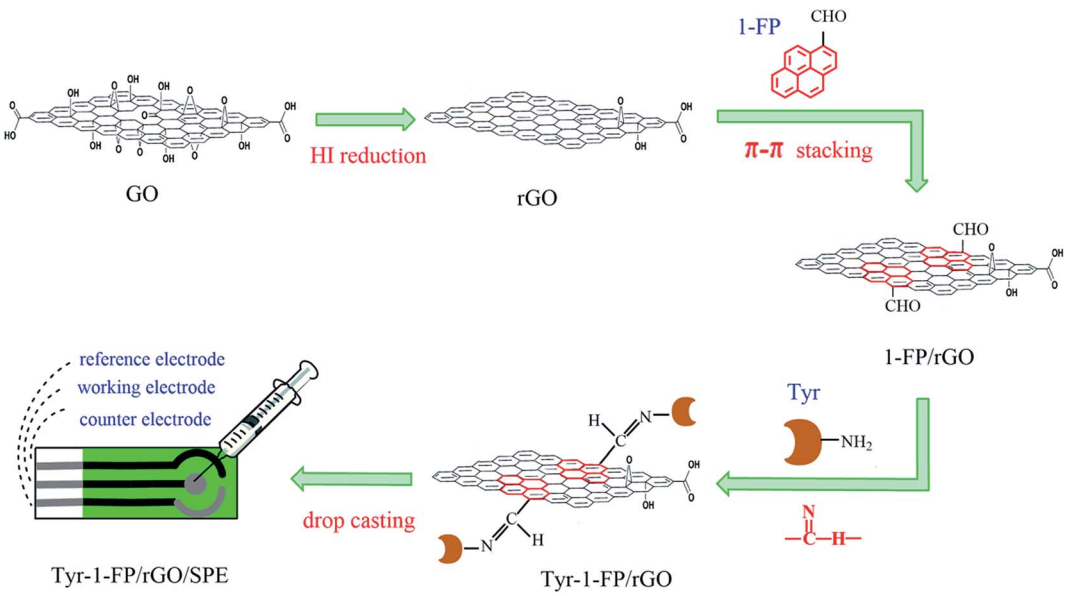

Scheme 1 Schematic representation of assembly for Tyr-1-FP/rGO/SPE electrode.

scans at a resolution of 4 cm^{-1}. XPS was obtained with an AXIS-Ultra instrument from Kratos Analytical using monochromatic Al Kα radiation (225 W, 15 mA, 15 kV) and low-energy electron flooding for charge compensation. The EIS measurements were performed in a 0.1 M KCl solution containing 5 mM $K_3[Fe(CN)_6]$ and $K_4[Fe(CN)_6]$, the results were plotted in the form of Nyquist plots with a frequency range from 0.01 Hz to 100k Hz.

2.3. Fabrication of Tyr-1-FP/rGO/SPE

Scheme 1 illustrates the schematic of the preparation of the Tyr-1-FP/rGO/SPE biosensor. First of all, rGO was obtained by the hydroiodic acid reduction of GO.[43] 10 mg rGO and 80 mg 1-FP were added into 100 mL absolute ethanol and mixed under ultrasonication for 2 h. After standing overnight at room temperature, the mixture was centrifuged and washed with ethanol for several times, and the resulted deposit was dried under 70 °C to obtain 1-FP/rGO composites.

In the procedure of enzyme immobilization, 1-FP/rGO was first dispersed in 0.1 M pH 7.0 PBS with the aid of ultrasonication to give a 2 mg mL^{-1} stable 1-FP/rGO suspension. After that, 2 mg mL^{-1} Tyr solution (dissolved in pH 7.0 PBS) was mixed with 2 mg mL^{-1} 1-FP/rGO suspension (1 : 1, v/v) and shaken for over 30 min to obtain a homogeneous 1-FP-Tyr/rGO suspension.

For fabrication of the Tyr-1-FP/rGO/SPE electrode, 10 μL of the Tyr-1-FP/rGO suspension was dropped onto the working electrode surface of SPE and the modified electrode was allowed to dry at 4 °C overnight. For comparison, rGO/SPE and 1-FP/rGO/SPE were fabricated with the similar procedures. All of the modified electrodes were stored at 4 °C in a refrigerator before use.

3. Results and discussion

3.1. Physicochemical characterization

3.1.1. FT-IR of 1-FP functionalized rGO. In order to confirm the successfully fabrication of 1-FP functionalized rGO. The structures of the rGO, 1-FP and 1-FP/rGO films were investigated using FTIR (Fig. 1). In rGO (Fig. 1a), we observe a strong and broad absorption at 3417 cm^{-1} due to O–H stretching vibration. Besides, the FTIR spectrum of rGO showed prominent absorption bands at 3417 cm^{-1} O–H stretching vibration 1625 cm^{-1} (for C=C stretching vibrations), 1075 cm^{-1} (for C–O stretching vibrations) and 2924, 2865 cm^{-1} (for C–H stretching vibration). Fig. 1b displays the spectrum of 1-FP, it can be seen that 1-FP spectrum is consisted of prominent bands of aldehyde group (2820, 2720 and 1703 cm^{-1}) and aromatic nucleus (1600, 1580, 1500, 1450 cm^{-1}). A series of peaks at 880, 840, 709 and 650 cm^{-1} in the spectrum are attributed to the C–H out of plane bending vibrations, and the peak at 3033 cm^{-1} is ascribed to the aromatic ring C–H stretching vibration. As shown in Fig. 1c, the spectrum of 1-FP/rGO is nearly the same as that obtained from the pure 1-FP, confirming the successful functionalization of rGO with 1-FP *via* the π–π interaction between the pyrenyl groups of 1-FP and the six-membered rings of rGO. Thus, the aldehyde groups should be distributed uniformly on the surface of rGO and the 1-FP–rGO composites provide a promising matrix for enzyme immobilization.

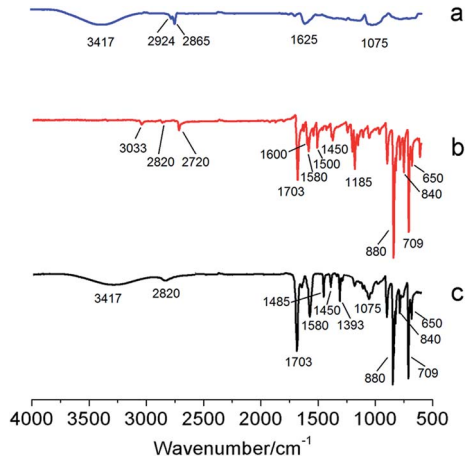

Fig. 1 FTIR spectra of rGO (a), 1-FP (b) and 1-FP/rGO (c).

3.1.2. XPS of Tyr-1-FP/rGO. XPS measurement was conducted here to confirm the preparation of Tyr-1-FP/rGO. As expressed in Fig. 2, the existence of N 1s is definitely attributed to Tyr, demonstrating that Tyr had been successfully linked to 1-FP/rGO. Moreover, the –C=N at 399.8 eV is most likely due to the condensation reaction between Tyr and 1-FP, which further confirms the successful immobilization of Tyr.

Additionally, other XPS peaks of Tyr-1-FP/rGO were also demonstrated in Fig. S1 (ESI†). The C 1s spectrum of the Tyr-1-FP/rGO reveals that it consists of two main components originating from the C–O (~286.1 eV) and C=C/C–C (~284.6 eV) groups and three minor components from C–H (~283.9 eV), C=N (~287.0 eV) and O–C=O (~288.1 eV) groups. For comparison purpose, the C 1s spectrum of the 1-FP/rGO was presented in Fig. S2 (ESI†). As shown, the C=O bond exists mainly due to aldehyde groups that was distributed uniformly on the rGO surface. While after interact with enzyme, the C=N peak was observed instead of C=O, indicating the successful condensation reaction between aldehyde groups of 1-FP/rGO and amino groups of Tyr. Moreover, the Cu spectrum of the Tyr-1-FP/rGO further confirms the successful immobilization of enzyme although the Cu peaks aren't very high-resolution

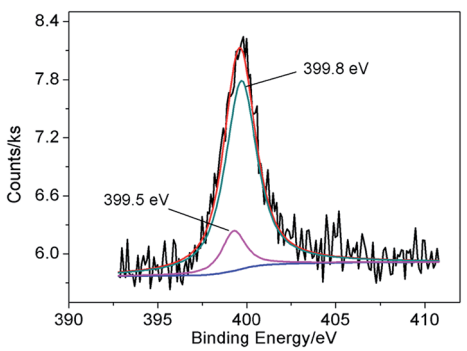

Fig. 2 XPS spectrum of the Tyr-1-FP/rGO: high resolution scan for N 1s.

(Fig. S1D in ESI†), which maybe because the copper sites of redox center in biomolecules is usually embedded deeply into the large three dimensional structures of enzyme molecules.

3.1.3. Characterization of Tyr-1-FP/rGO/SPE. EIS was applied to monitor the whole procedure in preparing Tyr-1-FP/rGO modified electrodes, which could provide useful information between each step and often be used to study the surface features of modified electrodes.[44] A typical impedance spectrum consists of a semicircle portion observed at a high frequency range corresponding to the electron-transfer-limited process and a linear portion at low frequencies representing the diffusion-limited process. The electron transfer resistance (R_{ct}) at the electrode surface can be quantified using the diameter of the semicircle. Fig. 3 presents the representative impedance spectra of bare SPE, rGO/SPE, 1-FP/rGO/SPE and Tyr-1-FP/rGO/SPE in 0.1 M KCl solution containing 5 mM $[Fe(CN)_6]^{3-/4-}$. To understand clearly the electrical properties of the electrodes/solution interfaces, the Randle's equivalent circuit (inset of Fig. 3) was chosen to fit the obtained impedance data.[45] In the Randle's circuit, R_{ct}, W, C_{dl} and R_{sol} represent the charge transfer resistance, the diffusion impedance, the interfacial capacity and the electrolyte resistance, respectively. It was assumed that R_{ct} and W were both in parallel to C_{dl}. This parallel combination of R_{ct} and C_{dl} gives rise to a semicircle in the complex plane plot of Z'' against Z', and the semicircle diameter equals the charge transfer resistance (R_{ct}). This resistance exhibits the electron transfer kinetics of the redox probe at electrode interface. As shown in Fig. 3, a well-defined semicircle curve was observed with each modified electrode. The R_{ct} values of rGO/SPE (Fig. 3b), 1-FP/rGO/SPE (Fig. 3c) and Tyr-1-FP/rGO/SPE (Fig. 3d) were much lower than that of bare the SPE electrode (Fig. 3a), indicating that the introduction of rGO can greatly improve the conductivity of electrode. After 1-FP stacked onto rGO, a bigger semicircle at high frequencies was obtained, indicating that the electron transfer of the redox probe was obstructed. Moreover, an obvious increase in the interfacial resistance was observed when Tyr was immobilized in 1-FP/rGO, the increase of R_{ct} might have been caused by the hindrance of the macromolecular structure of Tyr to the electron transfer. The results of EIS analysis also support that the Tyr-1-FP/rGO had been successfully fabricated and modified onto the SPE surface.

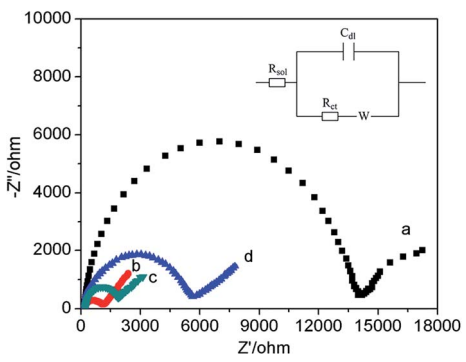

Fig. 3 AC impedance spectrum of (a) bare SPE, (b) rGO/SPE, (c) 1-FP/rGO/SPE and (d) Tyr-1-FP/rGO/SPE in 5 mM $K_3[Fe(CN)_6]/K_4[Fe(CN)_6]$ (1 : 1) containing 0.1 M KCl solution. The frequency range was from 0.01 Hz to 100k Hz. The amplitude potential was 5 mV. Inset, the Randle's equivalent circuit for EIS analysis.

3.2. Optimization of preparation parameters

To optimize the mass ratio between 1-FP and rGO ($R_{1\text{-FP/rGO}}$), 1-FP/rGO composites with five kinds of mass ratio (1/32, 1/16, 1/8, 1/4 and 1/2) were prepared in this paper. The electrochemical performance of Tyr-1-FP/rGO/SPE electrodes with different $R_{1\text{-FP/rGO}}$ values have been investigated by CV in O_2-saturated PBS buffer solution with 100 μM phenol, and the histograms about the value of reduction peak current (I_{pc}) against $R_{1\text{-FP/rGO}}$ are presented in Fig. 4A. As shown in Fig. 4A, significant increases of I_{pc} were observed from $R_{1\text{-FP/rGO}} = 1/32$ to 1/8, while I_{pc} at $R_{1\text{-FP/rGO}} = 1/8$ is nearly as high as that at $R_{1\text{-FP/rGO}} = 1/4$ and 1/2. These results indicate that 1-FP is favorable for the immobilization of Tyr onto rGO, and the six-membered rings of rGO might have been stacked completely by 1-FP in the case of $R_{1\text{-FP/rGO}} = 1/8$. Therefore, we choose 1/8 as the optimum value of $R_{1\text{-FP/rGO}}$ in the experiments carried out in this paper.

To obtain the optimum amount of added enzyme, 1 mL of various concentrations of Tyr was added into 1 mL of 2 mg mL^{-1} 1-FP/rGO suspension, which was subsequently shaken for over 30 min to obtain 1-FP-Tyr/rGO suspension. As shown in Fig. 4B, the current response of phenol increased with increasing concentration of Tyr and reached a maximum at 2 mg mL^{-1}, thereafter the current response decreased significantly. This could be presumed that the covalent bonding of Tyr with 1-FP/rGO was saturated at 2 mg mL^{-1}, higher amount of added enzyme leads to excess Tyr exists in the electrolyte solution. These free Tyr molecules would increase the hydrophobicity of the electrode surface and make the electron transfer more difficult. Therefore, 2 mg mL^{-1} Tyr was chosen for all subsequent experiments.

3.3. Cyclic voltammetric behaviors of phenol

Fig. 5 displays the typical CVs of phenol in O_2-saturated 0.1 M PBS (pH 7.0) at SPE, rGO/SPE, 1-FP–rGO/SPE and Tyr-1-FP/rGO/SPE. As demonstrated, there was no obvious redox peak in the potential range of −0.6–0.6 V on the modified electrodes without Tyr (Fig. 5a–c). However, a distinct reduction peak −0.08 V was observed with Tyr-1-FP/rGO/SPE (Fig. 5d), which was due to the reduction of *o*-quinone produced from the enzymatic reaction on the electrode surface. Besides, the high currents at the very negative potential is most possibly due to oxygen reduction at the electrode surface.[46]

The electrocatalytic activity of Tyr-1-FP/rGO/SPE electrode towards phenol is examined by CV analysis. Fig. 6A compares the CVs of the Tyr-1-FP/rGO/SPE in the N_2-saturated (curve a), air-saturated (curve b) and O_2-saturated (curve c) PBS buffer solution with 50 μM phenol. It can be seen that no obvious peaks was observed in the solution saturated with N_2, while a prominent cathodic wave at −0.08 V appeared in both air-saturated and O_2-saturated phenol solution, indicating a typical electrocatalytic oxidation of phenols by Tyr occurs, when oxygen accepts the electron that phenols lost at Tyr.

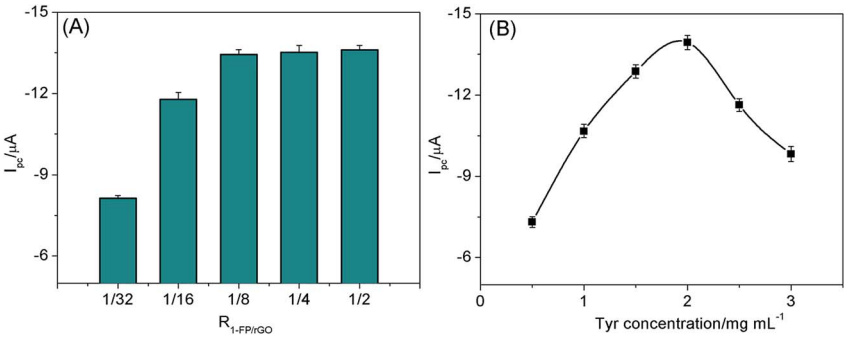

Fig. 4 Effect of the mass ratio of 1-FP to rGO (A) and Tyr concentration (B) on the reduction response of Tyr-1-FP/rGO/SPE electrode in O_2-saturated PBS (pH 7.0) with 100 μM phenol.

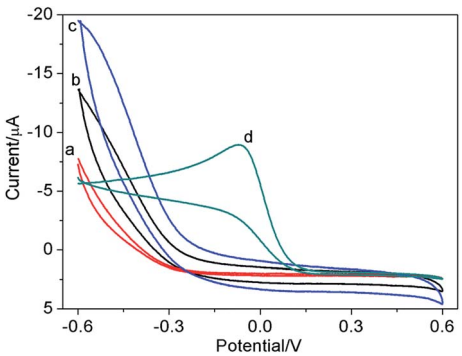

Fig. 5 CVs of (a) SPE, (b) rGO/SPE, (c) 1-FP/rGO/SPE and (d) Tyr-1-FP/rGO/SPE in O_2-saturated 0.1 M PBS (pH 7.0) containing 50 μM phenol at the scan rate of 100 mV s^{-1}.

The effect of pH value on the current response of the biosensor to 100 μM phenol was investigated with the pH range from 5 to 8 and the results were shown in Fig. 6B. It can be seen that the response current increased with the increase of pH from 5.0 up to 7.0, and then it decreased at higher pH. The maximum reduction peak was obtained at pH 7.0, which was in good accordance with those reported by others.[47–49] The decrease in the response current at pH values greater than 7.0 may be due to the involvement of protons in the reduction reaction of *o*-quinone, and at low pH the increase in amperometric response with an increasing pH is attributed to the increase of the enzyme activity.[49,50] Therefore, in order to achieve high sensitivity, pH 7.0 was chosen for the determination of phenols. In addition, with the increase of pH, the cathodic peak potential shifted negatively, and the linear relationship of the

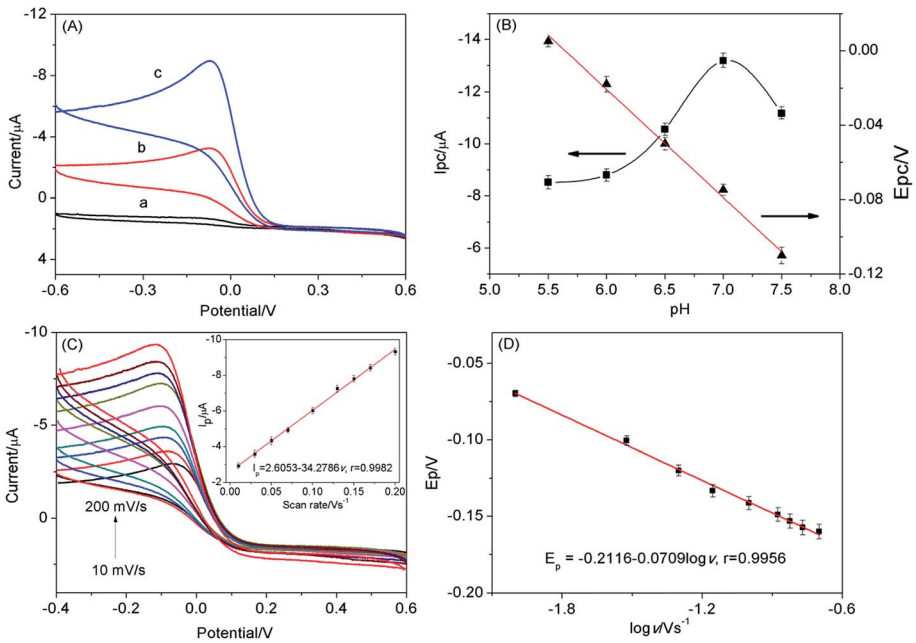

Fig. 6 (A) CVs of Tyr-1-FP/rGO/SPE in the (a–c) N_2-, air- and O_2-saturated PBS buffer solution (pH 7.0) containing 50 μM phenol at the scan rate of 50 mV s^{-1}; (B) effect of pH value on the response of 100 μM phenol; (C) CVs of 50 μM phenol at different scan rates: 10, 30, 50, 70, 100, 130, 150, 170 and 200 mV s^{-1}, inset is plot of the peak current *vs.* scan rate; (D) the relationship of peak potential (E_p) *vs.* the logarithm of scan rate (log *v*).

reduction potential (E_{pc}) as a function of pH was expressed as $E_{pc} = -0.0582pH + 0.3285$ ($r = 0.9917$, E_{pc} in V). This slope value of -58.2 mV pH^{-1} is close to the theoretical value of -59 mV pH^{-1}, indicating an equal number of protons and electrons participating in the electrochemical process.

Fig. 6C shows the CVs of 50 μM phenol in PBS (pH 7.0) at the Tyr-1-FP/rGO/SPE electrode with various scan rates ranging from 10 mV s^{-1} to 200 mV s^{-1}. It was found that the cathodic peak current of phenol increased linearly with increasing scan rate (inset of Fig. 6C), suggesting that the reduction of phenol at Tyr-1-FP/rGO/SPE electrode is an irreversible surface-controlled process. The relationship between the reduction peak potential (E_{pc}) and the logarithm of scan rate ($\log v$) for the electrocatalysis of phenol on the fabricated Tyr-1-FP/rGO/SPE is also shown in Fig. 6D. As can be seen, $\log v$ is proportional to E_{pc} within the range of 10–200 mV s^{-1}, and the equation can be expressed as: $E_{pc} = -0.0709 \log v - 0.2166$ ($r = 0.9956$, E_{pc} in V, v in mV s^{-1}). As for an adsorption-controlled and totally irreversible electrode process, the slope of the linear regression equations is equal to $-2.303RT/\alpha nF$. Here, R is the thermodynamic gas constant (8.314 J K^{-1} mol^{-1}), F is the Faraday constant (96 500 C mol^{-1}), T represents temperature (298 K), n is the electron transfer number and α is the charge transfer coefficient. According to Laviron equation,[45] αn is calculated to be 0.84. Generally, α is assumed to be 0.5 in totally irreversible electrode process, so n is around 2. Because the number of electrons and protons involved in the reduction process was equal in this work, the electrochemical reduction of phenol at the electrode is a two-electron and two-proton process. Therefore, the electro-reduction mechanism of phenol at Tyr-1-FP/rGO/SPE can be expressed as Scheme 2.

3.4. Electrochemical determination of phenol

Fig. 7 displays DPVs of phenol with different concentrations from 0.5 to 150 μM obtained at the Tyr-1-FP/rGO/SPE biosensor. As can be seen, the cathodic peak current increases linearly with increasing phenol concentration (inset of Fig. 7; linear regression equation: I (μA) $= -0.1131C_{DA}$ (μM) $- 3.4312$, $R^2 = 0.9975$). Detection limit of this sensor was calculated to be 0.17 μM (S/N = 3). This excellent performance of the proposed electrode could be ascribed to the high electrocatalytic activity of Tyr immobilized onto 1-FP/rGO surface. Table 1 compares the detection of phenol by Tyr-1-FP/rGO/SPE with other electrochemical sensors. It is evident that the Tyr-1-FP/rGO/SPE biosensor exhibited superiority over some earlier reported sensors towards sensitive determination of phenol. This excellent performance of the proposed biosensor could be ascribed to efficient immobilization of Tyr to 1-FP/rGO and outstanding conductivity of rGO as well as the high bioactivity of Tyr retained by 1-FP/rGO.

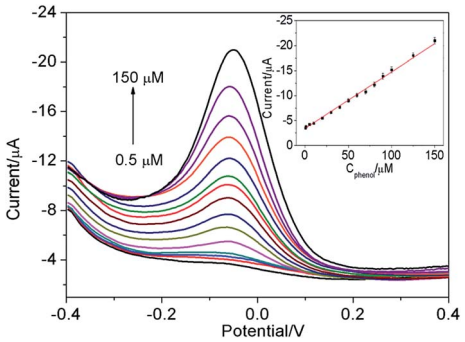

Fig. 7 DPV curves obtained at Tyr-1-FP/rGO/SPE in 0.1 M PBS (pH 7.0) containing different concentrations of phenol: 0.5, 1, 5, 10, 20, 30, 40, 50, 60, 70, 80, 90, 100, 125 and 150 μM (from bottom to top). Inset, plot of current response *vs.* the concentration of phenol.

3.5. Reproducibility and stability of Tyr-1-FP/rGO/SPE

The repeatability of the same Tyr-1-FP/rGO/SPE described above was evaluated by the detection of 20 μM phenol. A relative standard deviation (R.S.D.) value of 2.14% was obtained for ten successive determinations, indicating that this electrode possessed good repeatability. The fabrication reproducibility

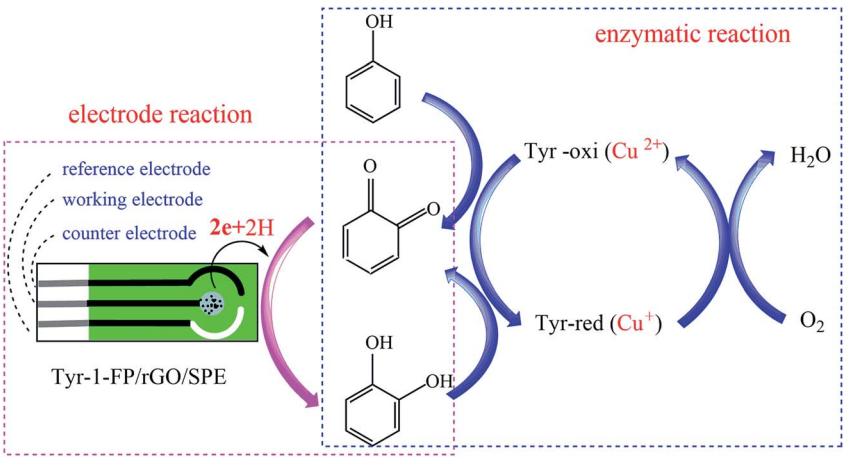

Scheme 2 Schematic representation of the biosensor and its different parts, also the scheme depicts enzymatic reaction between Tyr and phenol with electrochemical reduction of the quinone formed at the biosensor surface. Tyr-oxi: oxidized form of Tyr-and Tyr-red: reduced form of Tyr.

Table 1 Comparison of different sensors for the detection of DA

Sensor	Linear range (μM)	Detection limit (μM)	Sensitivity	References
PPO/PTS-PPY/GCP[a]	3.3–220.3	—	17.1 μA mM^{-1}	51
MWCNT/DTDAB/Tyr-NCPE[b]	1.5–25	—	2900 μA mM^{-1}	52
Tyr/$MgFe_2O_4$–SiO_2/CPE[c]	1–250	0.6	54.2 μA mM^{-1}	53
Layered PANI sheets electrode[d]	20–80	4.43	1485.3 μA mM^{-1} cm^{-2}	54
Tyr-ZnO-BDND[e]	1–150	0.2	287.1 μA mM^{-1} cm^{-2}	55
Ni/Al LDH on Pt[f]	5–650	5	155 μA mM^{-1}	56
Tyr-1-FP/rGO/SPE	0.5–150	0.17	113.1 μA mm^{-1}, 1615.7 μA mM^{-1} cm^{-2}	This work

[a] Tyrosinase/*p*-toluene sulfonate ion-doped polypyrrole/glassy carbon plate. [b] Multiwall carbon nanotube/dimethylditetradecylammonium bromide/tyrosinase-carbon paste electrode. [c] Tyrosinase modified core–shell magnetic nanoparticles supported at a carbon paste electrode. [d] Layered polyaniline nanosheets electrode. [e] Tyrosinase-biofunctional ZnO nanorod microarrays on the boron-doped nanocrystalline diamond substrates. [f] Ni/Al layered double hydroxide thin films deposited on Pt electrodes.

was evaluated with five electrodes prepared under the same conditions. The R.S.D. was calculated to be 3.82%, which demonstrated the reliability of the fabrication procedure.

The long-term stability of the Tyr-1-FP/rGO/SPE electrode was evaluated by measuring its response to 20 μM phenol for 2 months. When not in use, the electrode was stored at 4 °C. Its current response was tested every 3 days during the first month. Beyond this period, the experiment was carried out once per 10 days. The electrode remained about 85% of its initial response after 1 month, and decreased gradually to about 62% after 2 months. Such a favorable stability could be attributed to the effective covalent immobilization method.

3.6. Analytical applications

To verify the actual feasibility of the proposed sensor, Tyr-1-FP/rGO/SPE was applied to determine phenol added to natural waters (Table 2). The percentage of the recovery values was calculated by comparing the concentration obtained from the proposed electrode with that obtained from HPLC. It was found that the recoveries were in the range of 97.54% to 102.22%, indicating that the proposed Tyr-1-FP/rGO/SPE could be used for the detection of phenol in real samples.

Table 2 Determination of added phenol in natural waters[a]

Water sample	Added (μM)	Found by proposed sensor (μM)	Found by HPLC (μM)	Recovery (%)
A	10	9.92	10.17	97.54
	50	49.81	50.14	99.34
	100	98.73	100.28	98.45
B	10	10.01	10.14	98.72
	50	50.87	49.92	101.90
	100	100.11	101.23	98.89
C	10	9.79	10.02	97.70
	50	51.09	49.98	102.22
	100	99.89	98.25	101.67
D	10	10.03	10.24	97.95
	50	48.98	49.62	98.71
	100	98.97	99.12	99.85

[a] A, Taihu Lake; B, Yangtze River; C, Yellow Sea of Yancheng region; D, Qinhuai River.

4. Conclusions

In summary, we reported the first use of 1-FP as a bifunctional molecule in rGO functionalization and enzyme immobilization. Using this method, we successfully fabricated Tyr-1-FP/rGO/SPE biosensor. The biosensor provides a suitable microenvironment for retaining bioactivity of Tyr due to the flexible aldehyde chain of 1-FP. The resulted biosensor exhibited good analytical performance to phenol in terms of wide linear range, low detection limit, high sensitivity and good stability. Practical application in the determination of phenol in real waters was also succeeded with satisfying results indicated that the biosensor we prepared had a great potential for practical application.

Acknowledgements

The authors gratefully acknowledge the support provided by special fund of Specialized Research Fund for the Doctoral Program of Higher Education (20130094120009), National Natural Science Foundation of China (Grant No. 51308183, 51179052), Natural Science Foundation of Jiangsu Province of China (Grant No. BK20130828), the Fundamental Research Funds for the Central Universities (2013B32214, 2014B07414, 2015B36414), Jiangsu Province Ordinary University Graduate Student Scientific Research Innovation Project (KYLX15_0475) and A Project Funded by the Priority Academic Program Development of Jiangsu Higher Education Institutions.

Notes and references

1 L. Lu, L. Zhang, X. Zhang, S. Huan, G. Shen and R. Yu, *Anal. Chim. Acta*, 2010, **665**, 146–151.
2 C. Medina-Plaza, C. García-Cabezón, C. García-Hernández, C. Bramorski, Y. Blanco-Val, F. Martín-Pedrosa, T. Kawai, J. A. de Saja and M. L. Rodríguez-Méndez, *Anal. Chim. Acta*, 2015, **853**, 572–578.

3 R. Aghav, S. Kumar and S. Mukherjee, *J. Hazard. Mater.*, 2011, **188**, 67–77.
4 A. Schieber, P. Keller and R. Carle, *J. Chromatogr. A*, 2001, **910**, 265–273.
5 A. Edelmann, J. Diewok, K. C. Schuster and B. Lendl, *J. Agric. Food Chem.*, 2001, **49**, 1139–1145.
6 M.-C. Monje, C. Privat, V. Gastine and F. Nepveu, *Anal. Chim. Acta*, 2002, **458**, 111–117.
7 C. D. Chriswell, R. C. Chang and J. S. Fritz, *Anal. Chem.*, 1975, **47**, 1325–1329.
8 S. Pérez-Magariño, I. Revilla, M. González-SanJosé and S. Beltrán, *J. Chromatogr. A*, 1999, **847**, 75–81.
9 F. Karim and A. N. M. Fakhruddin, *Rev. Environ. Sci. Bio/Technol.*, 2012, **11**, 261–274.
10 E. Han, Y. Yang, Z. He, J. Cai, X. Zhang and X. Dong, *Anal. Biochem.*, 2015, **486**, 102–106.
11 E. Çevik, M. Şenel, A. Baykal and M. F. Abasıyanık, *Sens. Actuators, B*, 2012, **173**, 396–405.
12 L. Campanella, G. Favero, M. P. Sammartino and M. Tomassetti, *Talanta*, 1994, **41**, 1015–1023.
13 C. A. Ramsden and P. A. Riley, *Bioorg. Med. Chem.*, 2014, **22**, 2388–2395.
14 Z. Fan, Q. Lin, P. Gong, B. Liu, J. Wang and S. Yang, *Electrochim. Acta*, 2015, **151**, 186–194.
15 R. Devi and C. Pundir, *Sens. Actuators, B*, 2014, **193**, 608–615.
16 Z.-G. Wang, L.-S. Wan, Z.-M. Liu, X.-J. Huang and Z.-K. Xu, *J. Mol. Catal. B: Enzym.*, 2009, **56**, 189–195.
17 R. Fernandez-Lafuente, P. Armisén, P. Sabuquillo, G. Fernández-Lorente and J. M. Guisán, *Chem. Phys. Lipids*, 1998, **93**, 185–197.
18 H. du Toit and M. Di Lorenzo, *Electrochim. Acta*, 2014, **138**, 86–92.
19 Q. Liu, A. Fei, J. Huan, H. Mao and K. Wang, *J. Electroanal. Chem.*, 2015, **740**, 8–13.
20 C. Di Bari, S. Shleev, A. L. De Lacey and M. Pita, *Bioelectrochemistry*, 2016, **107**, 30–36.
21 R. R. Dutta and P. Puzari, *Biosens. Bioelectron.*, 2014, **52**, 166–172.
22 E. Voitechovič, A. Bratov, N. Abramova, J. Razumienė, D. Kirsanov, A. Legin, D. Lakshmi, S. Piletsky, M. Whitcombe and P. Ivanova-Mitseva, *Electrochim. Acta*, 2015, **173**, 59–66.
23 T. Itoh, T. Shimomura, A. Hayashi, A. Yamaguchi, N. Teramae, M. Ono, T. Tsunoda, F. Mizukami, G. D. Stucky and T. A. Hanaoka, *Analyst*, 2014, **139**, 4654–4660.
24 H. Ciftci, Y. Oztekin, U. Tamer, A. Ramanaviciene and A. Ramanavicius, *Colloids Surf., B*, 2014, **123**, 685–691.
25 H. L. Pang, J. Liu, D. Hu, X. H. Zhang and J. H. Chen, *Electrochim. Acta*, 2010, **55**, 6611–6616.
26 W. Song, D. W. Li, Y. T. Li, Y. Li and Y.-T. Long, *Biosens. Bioelectron.*, 2011, **26**, 3181–3186.
27 Z. Taleat, A. Khoshroo and M. Mazloum-Ardakani, *Microchim. Acta*, 2014, **181**, 865–891.
28 A. Michopoulos, A. Kouloumpis, D. Gournis and M. I. Prodromidis, *Electrochim. Acta*, 2014, **146**, 477–484.
29 F. J. V. Gomez, A. Martín, M. F. Silva and A. Escarpa, *Microchim. Acta*, 2015, 1–7.
30 F. Valentini, E. Ciambella, V. Conte, L. Sabatini, N. Ditaranto, F. Cataldo, G. Palleschi, M. Bonchio, F. Giacalone and Z. Syrgiannis, *Biosens. Bioelectron.*, 2014, **59**, 94–98.
31 S. Cinti, S. Politi, D. Moscone, G. Palleschi and F. Arduini, *Electroanalysis*, 2014, **26**, 931–939.
32 P. Niu, C. Fernández-Sánchez, M. Gich, C. Navarro-Hernández, P. Fanjul-Bolado and A. Roig, *Microchim. Acta*, 2015, 1–7.
33 R. Antiochia and L. Gorton, *Sens. Actuators, B*, 2014, **195**, 287–293.
34 M. Sahin and E. Ayranci, *Electrochim. Acta*, 2015, **166**, 261–270.
35 A. K. Geim and K. S. Novoselov, *Nat. Mater.*, 2007, **6**, 183–191.
36 A. C. Neto, F. Guinea, N. Peres, K. S. Novoselov and A. K. Geim, *Rev. Mod. Phys.*, 2009, **81**, 109.
37 S. Zhou, D. Wei, H. Shi, X. Feng, K. Xue, F. Zhang and W. Song, *Talanta*, 2013, **107**, 349–355.
38 X. H. Zhou, L. H. Liu, X. Bai and H.-C. Shi, *Sens. Actuators, B*, 2013, **181**, 661–667.
39 Y. Yan, M. Zhang, K. Gong, L. Su, Z. Guo and L. Mao, *Chem. Mater.*, 2005, **17**, 3457–3463.
40 L. C. Tang, Y. J. Wan, D. Yan, Y. B. Pei, L. Zhao, Y. B. Li, L. B. Wu, J. X. Jiang and G. Q. Lai, *Carbon*, 2013, **60**, 16–27.
41 D. Zhou, Q. Y. Cheng and B. H. Han, *Carbon*, 2011, **49**, 3920–3927.
42 M. Ayán-Varela, J. I. Paredes, S. Villar-Rodil, R. Rozada, A. Martínez-Alonso and J. M. D. Tascón, *Carbon*, 2014, **75**, 390–400.
43 S. Pei, J. Zhao, J. Du, W. Ren and H.-M. Cheng, *Carbon*, 2010, **48**, 4466–4474.
44 S. Su, H. Sun, F. Xu, L. Yuwen, C. Fan and L. Wang, *Microchim. Acta*, 2014, **181**, 1497–1503.
45 H. O. Finklea, D. A. Snider, J. Fedyk, E. Sabatani, Y. Gafni and I. Rubinstein, *Langmuir*, 1993, **9**, 3660–3667.
46 H. Notsu, T. Tatsuma and A. Fujishima, *J. Electroanal. Chem.*, 2002, **523**, 86–92.
47 L. Lu, L. Zhang, X. Zhang, S. Huan, G. Shen and R. Yu, *Anal. Chim. Acta*, 2010, **665**, 146–151.
48 G. Bayramoglu, A. Akbulut and M. Y. Arica, *J. Hazard. Mater.*, 2013, **244–245**, 528–536.
49 S. Liu, J. Yu and H. Ju, *J. Electroanal. Chem.*, 2003, **540**, 61–67.
50 S. Hashemnia, S. Khayatzadeh and M. Hashemnia, *J. Solid State Electrochem.*, 2012, **16**, 473–479.
51 Z. H. Rajesh, W. Takashima and K. Kaneto, *React. Funct. Polym.*, 2004, **59**, 163–169.
52 S. Hashemnia, S. Khayatzadeh and M. Hashemnia, *J. Solid State Electrochem.*, 2011, **16**, 473–479.
53 Z. Liu, Y. Liu, H. Yang, Y. Yang, G. Shen and R. Yu, *Anal. Chim. Acta*, 2005, **533**, 3–9.
54 H. K. Seo, S. Ameen, M. S. Akhtar and H. S. Shin, *Talanta*, 2013, **104**, 219–227.
55 J. Zhao, D. Wu and J. Zhi, *Bioelectrochemistry*, 2009, **75**, 44–49.
56 E. Scavetta, A. Casagrande, I. Gualandi and D. Tonelli, *J. Electroanal. Chem.*, 2014, **722–723**, 15–22.

